Numerical and experimental assessment of a large industrial thrust bearing

Benjamin DEFOY*, Xavier DE LEPINE**, Lionel BROUSSARD*** and Mohamed OSAMA****

*Turbomachinery Solutions, GE Oil & Gas
480 Allée G. Eiffel, 71200 Le Creusot, France
E-mail: benjamin.defoy@ge.com
**Rotating Machines Dept., GE Energy Power Conversion
442 Rue de la Rompure, 54250 Champigneulles, France
***Control & Automation Technologies, GE Energy Power Conversion
18 Avenue du Québec, 91140 Villebon-sur-Yvette, France
****GE Global Research
Freisinger Landstrasse 50 D-85748 Garching, Germany

Abstract

Nowadays, Active Magnetic Bearings (AMB) are widely utilized in different industrial applications. Several applications have been successfully implemented in the field of Turbomachinery especially for large centrifugal compressors. These machines are subjected to high axial transient loads due to process operations. Considered simpler than radial bearings, the thrust bearing optimization has been largely neglected. Consequently, the thrust bearing suffers from sizing difficulties that lead to bad overall system optimization. Thrust behavior exhibits several peculiarities mainly due to the specific arrangement of thrust actuator made with a solid disk instead of laminated sheets for radial bearings. The work presented here aims to improve the prediction of thrust dynamic in order to better size this component and ensure smooth operation of machinery. The paper describes the complete analysis of a 25kN thrust bearing. The study is divided in two sections, first the actuator analysis and then the dynamic behavior of the complete system. The thrust bearing electromagnetic design was developed with the aid of Finite Element Analysis (FEA). The thrust bearing performance calculations are disclosed in this paper and compared with those of an actuator characterization test bench. Later, the thrust actuator is mounted on a complete AMB experimental set-up, equipped with a 200 kg rotor on two radial magnetic bearings. The test rig is equipped with a contactless axial actuator that enables the excitation of the rotor with different axial force amplitudes and ramps. The first FEA and experimental results are used to feed a simplified model of the complete thrust bearing. The experimental results are compared with numerical ones. The different phenomena observed are discussed and the system limitations are highlighted. This study enables better understanding of the behavior of large thrust bearings. In addition, the work realized help to predict and optimize thrust bearing response for each machine.

Keywords : Magnetic thrust, Transient dynamic, Numerical prediction, Experimental, Turbomachinery

1. Introduction

Due to the progress made in electronics, AMBs are now widely used in different industrial applications and have been successfully implemented in the field of turbomachinery (Maslen, 2008), (Ransom, et al., 2009), (Swan, et al., 2008). Their main advantages are that they provide a contact-less working environment, no sealing constraints, frictionless suspension, and that they constitute an active system (Schweitzer and Maslen, 2009). On the other hand, AMBs produce only electromagnetic attraction and have nonlinear characteristics; therefore AMBs are inherently unstable and require feedback control to ensure stable operation (Defoy, et al., 2014).

Several studies have been devoted to the elaboration of thrust models that enable a better understanding of actuator

behavior. Zhu and Knospe (2010) have proposed an analytical model of eddy current effect. The model helps for the prediction of the actuator bandwidth and thus for the analysis of the thrust dynamic behavior. Allaire et al. (1997) have experimentally studied the static and dynamic relation between current and force applied by a thrust magnetic bearing. They have pointed out the effects of eddy current and magnetic hysteresis. Jang et al. (2008) have studied an active thrust bearing of small size from design to experimental tests. Nevertheless, the understanding of thrust bearing is still unsatisfying compared to what has been done on radial magnetic bearings. The thrust bearing suffers from sizing difficulties leading to bad overall machine optimization.

On the other hand, some researches are exploring thrust bearing system optimization. Whitlow et al. (2014) have studied the effect of segmented actuators showing that a small number of cuts enable a significant improvement of the thrust bandwidth. Hijikata et al. (2008) have studied a different thrust arrangement to overcome usual thrust characteristics. Here, the work is realized on classical industrial arrangement with a solid disk on the rotor and annular electromagnets attached to the stator facing the both sides of the disk. This choice was dictated by the wish to better understand actual system limitations before going to improvements that can turn out to be costly and not necessary for all machines.

Industrial requirements involve several constraints regarding performance, robustness, easiness of integration and final controller tuning. These requirements are dictated by international standards such as ISO 14839 and API 617. The specifications of the final users must also be taken into account. The spectrum of applications covered by AMBs is nowadays largely diversified. For a centrifugal compressor, inherent disturbances are generated by common machine operations as gas flow evolution or incidents as triggered trip, power failure or equipment faults. These events lead to fast transient axial loads that must be properly managed by the magnetic thrust.

Thrust design must take into consideration process loads but without excessive margins as oversizing can limit the compressor operating capabilities. For example, a large thrust disk can limit the rotating speed due to peripheral speed constrain. Moreover, a large thrust disk contributes to reduce rotor bending frequencies and so the separation margins with critical speeds. In addition, large thrust capabilities can turn out to be not exploitable as it will be demonstrated in this article.

The work presented here aims to improve the understanding of large thrust bearing behavior. The 25kN thrust studied is large enough to be representative of real industrial magnetic thrust. The thrust is considered a SISO system with feedback loop on position signal.

The paper is divided into several sections. First, the thrust design is described, and then the FEA approach. Then, experimental measurement of force versus current are compared with prediction. The dynamic tests are then described together with the simplified model of the complete system. In this works, the transient response of the system submit to an external force is experimentally assessed and compared to the result obtained thanks to the numerical model of the system. Finally, the thrust performances and limitations are highlighted and the conclusions are summarized in the final section.

2. Steady state thrust characteristics

2.1 25kN thrust design

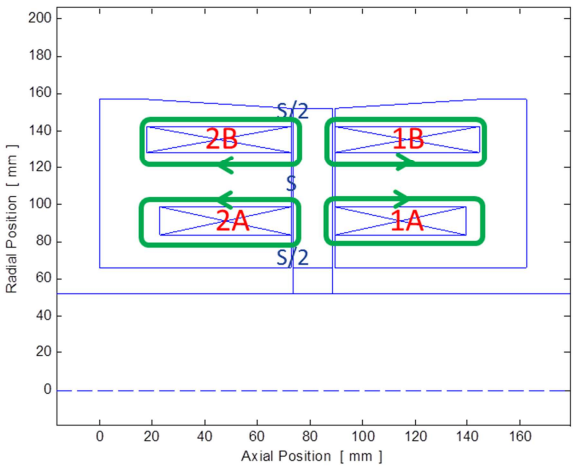

Fig. 1 Cross-section of E-core thrust bearing

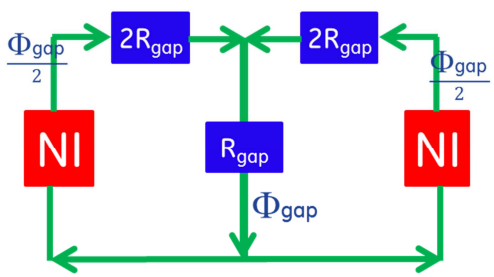

Fig. 2 Simplified magnetic circuit of E-core

The thrust bearing electromagnet actuator topology was chosen as an axisymmetric E-core to take advantage of its inherent flux path splitting, which allows for lower dimensions of both the stator back-iron and rotor disk thickness. Figure 1 shows a cross-section of an E-core electromagnet actuator with the main flux paths in green color. 1A is the inner coil for stator side 1 and 1B is the outer coil for stator side 1. Likewise, 2A is the inner coil for stator side 2 and 2B is the outer coil for stator side 2. Due to the design, the current in coils 1A and 1B and respectively for coils 2A and 2B are equal. Figure 2 shows a magnetic circuit for one side of the E-core electromagnet actuator. This magnetic circuit is simplified by neglecting all reluctances except those associated with the air-gaps. Note from Fig. 1 that the air-gap reluctance is defined as $R_{gap} = \frac{g}{\mu_0 S}$. S is the surface area of the middle tooth in the E-core, which is equal to twice the area of each of the outer teeth. N is the number of turns per coil, hence NI is the ampere-turn per coil. Φ_{gap} is the air-gap flux of the middle tooth.

2.2 Steady-state FEA analysis

Figure 3 shows the finite element analysis (FEA) results for a two dimensional magnetostatic model developed via the commercial software MagNet, for a current excitation only on stator side 1 coils; a current of 10A is applied in Fig. 3a and 15A in Fig. 3b. There is zero current excitation in stator side 2 coils. This current distribution represents an extreme case where the control current is equal to the bias current. 10A is the rated current of the electromagnetic actuator that results in its rated static force (25kN), while 15A is the rated current of the power converter supply, and hence represents the peak current capability of the thrust bearing system.

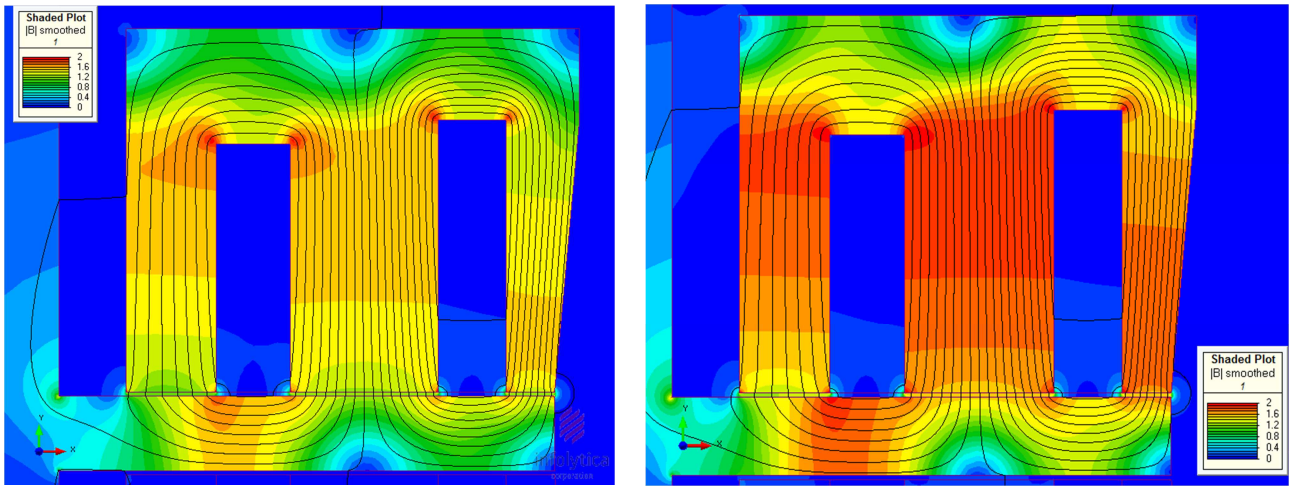

a) Current=10A b) Current=15A

Fig. 3 Steady-state FEA results for flux density and flux paths for a case of the rotor in the neutral position (equal air-gaps on both sides of the rotor disk): for rated current (a) the magnetic field is almost homogenous in the actuator whereas for maximum current available (b) magnetic field is saturated in the teeth area.

3. Static force characterization

3.1 Test set up presentation

In this section, the test setup that was used for the experimental validation of the FEA analysis is presented. The mechanical assembly is disclosed in Fig. 4. The parallelism between the floator and the stator is insured by using the frame as the reference. To this end, the parallelism between the disk and the frame is obtained at the manufacturing level. The internal screws of the cells are used to adjust the height of the stator and insure both the parallelism and the centring of the floator with respect of the stator. At this stage, the system can be clamped and used for both step response (one direction force only) and harmonic response (two directions force).

When the system is energized, the relative deformation of the floator with respect to the stator is monitored. Therefore, the evolution of the airgap can be used as an input for the numerical simulations.

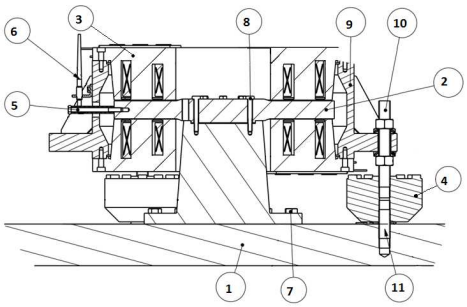

Fig. 4 Actuator force response characterization test rig. The disk (floator 2) is connected rigidly to the frame 1 through 7 and 8, while the stator of the actuator 3 is connected to the load cells 4 thanks to 9, 10 and 11. Conversely, the two parts of the stator are fixed together through an annular spacer 9 that guarantees the distance between them. A position sensor 6, fixed to the stator and targeting to an extension of the disk 5, allows the measurement of the relative deformation.

3.2 Step response

In a first step of validation, command current i_C is modulated from zero to maximum rated following different ramps. The bias current I_0 is set to its nominal value of 5A, both bottom and top magnets are energized and work together such that the total force generated by the actuators is linearized with respect to the command current. In that configuration, the currents of the actuators follow the rule described below by Eq. (1). For the dynamic analysis, FEA is conducted in transient time stepping.

$$i_{A1} = I_0 + i_C \; ; \; i_{A2} = I_0 - i_C \tag{1}$$

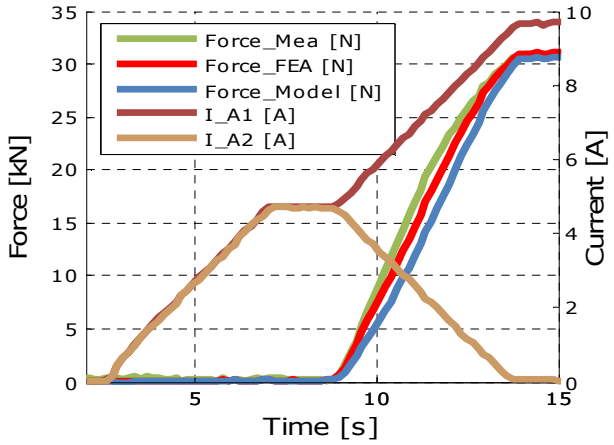

Fig. 5 Actuator response to 1A/s ramp, the ramp is sufficiently low to obtain established force at any time. The measured force is proportional to command current for values below 2A. Then nonlinearities appear, progressively the slope of force decreases.

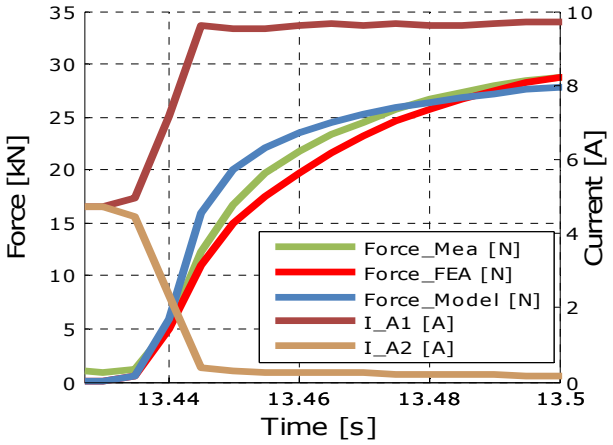

Fig. 6 Actuator response to 500A/s ramp, the response shows the effect of eddy currents: The force continues to increase whereas the current reaches its settled value. In the model, the eddy current characteristic frequency is settled to obtain the same initial slope.

Figure 5 shows the evolution of force with actuator currents when command current goes from 0 to 5A. On this test and the following the measured disk deflection is proportional to the force delivered and reaches a maximum value of 170µm. In order to take into consideration this effect, an equivalent disk translation is calculated and introduced in the numerical simulations. Due to disk displacement, the maximum force achieved exceeds the design of 25kN by 23%.

Figure 6 shows the same test configuration as Fig. 5 except for current ramp that equals 500A/s instead of 1A/s. The force slew rate is equal to 1.1MN/s at beginning, demonstrating good dynamic reactivity, and decrease progressively exhibiting eddy current effect.

Due to material experimental B/H characterization, the FEA analysis exhibits good correlation with experiments on all the tests.

3.3 Harmonic response

In this subsection, the dynamic response of the actuator is studied. The 5A bias current is activated and a harmonic current of 0.05A is added on top of it on the frequency range of 1 to 100Hz under the conditions of Eq. (2). As identified in step response the eddy current characteristic frequency is very low such that the actuator frequency bandwidth is very limited.

$$i_{A1} = i_0 + i_C \sin(2\pi f t)\ ;\ i_{A2} = i_0 - i_C \sin(2\pi f t) \tag{2}$$

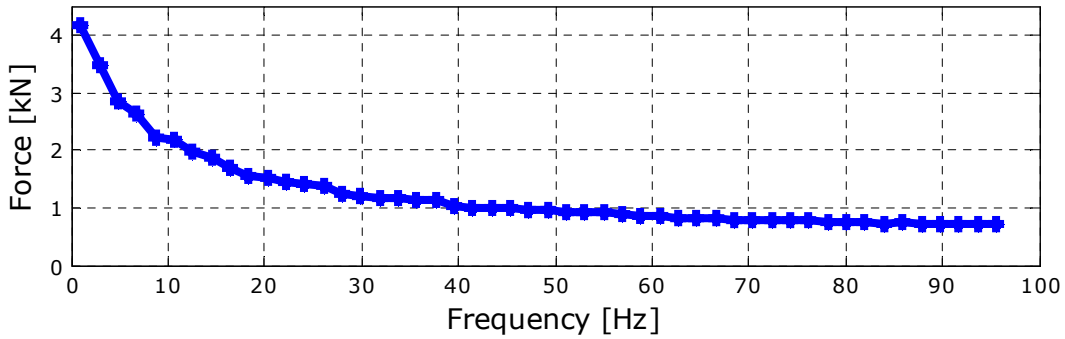

Fig. 7 Force response VS excitation frequency

4. Dynamic test description

4.1 Test rig

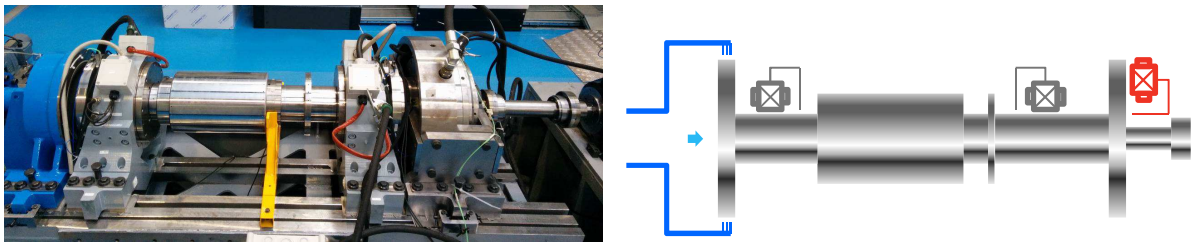

Fig. 8 System validation test rig. From left to right on the picture: axial pneumatic actuator, NDE radial magnetic bearing, speed sensor, DE radial magnetic bearing, tested thrust bearing and flexible coupling

Dynamic tests were conducted on a complete AMB experimental set-up, equipped with a 200 kg rotor on two identical radial AMBs called NDE (Non Drive End) and DE (Drive End) bearings as shown in Fig. 8. Bearings are powered in differential driving mode. Two displacement sensors are integrated in the housing of each bearing and are non-colocalised with actuators. The rotor test length is 1485mm from axial actuator to coupling. The thrust bearing is powered by an industrial control cabinet rated 15A/400V.

The test rig is equipped with a contactless axial pneumatic actuator that enables the excitation of the rotor with different axial force amplitudes and ramps. This pneumatic actuator is made of a pressurized vessel which one supplies through a control valve a small cavity (visible in blue in Fig. 8). This small cavity is closed thanks to a 280mm disk directly mounted on the test shaft. This disk is free of any contact with stator and a classical labyrinth seal enables management of gas leakages. The profile of the applied force is controlled by the vessel pressure and the supply valve opening parameters.

Thrust actuator is powered in differential driving mode with an internal current feedback loop. And, an axial displacement sensor is positioned in the space between shaft and electromagnet. The thrust bearing is controlled via a classical augmented PID controller that respects the requirement of applicable standards (Li, et al., 2006), (Spirig, et al., 2002). The system must control the rotor rigid supporting mode and 3 stator structural modes respectively at 32Hz 185Hz and 245Hz (see Fig. 10).

Tests were performed levitated, at zeros speed and in rotation up to 11000rpm. The high speed electrical motor is connected to the test shaft through a flexible coupling with negligible stiffness compare to magnetic bearing ones. As expected, no significant behavior modification was induced by rotor spinning. The rotation induced only measurement noise (harmonics) that lead to unavoidable control forces. These forces use a part of amplifier power and must be considered in the design in order to avoid any undesirable saturation effects.

4.2 System modelling

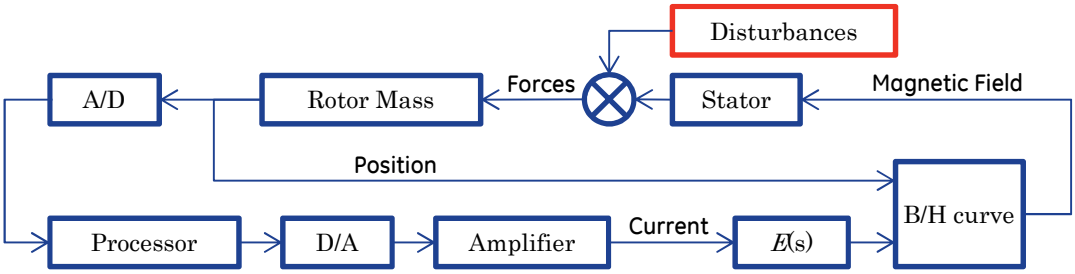

Fig. 9 Scheme of system model.

The FEA and experimental results are used to feed a simplified model of the complete bearing including actuator, amplifiers, sensors and control cabinet filters. The rotor is modelled as a single mass. The elements taken into consideration are the followings. Two eddy current sensors measure the rotor axial position, the analog signal is converted into digital by a high frequency Input/Output board with a not considered antialiasing filter. The I/O board makes a first signal processing with a second order Butterworth low pass filter (2.5kHz). Then, the I/O board communicates the rotor position at a rate of 5kHz to the system control processor. The bearing controller computes the adapted control current (here computation delay and ZOH are considered). The request current is sent to the I/O board and there filtered by a second order Butterworth low pass filter (5kHz) and converted into analog command signal. Finally, thrust actuator converts this request current into physical current and force.

For the electromagnet model, steel magnetic behavior has been measured on dedicated samples of metal. These tests have permitted the characterization of steel permeability and hysteresis loop. Hysteresis is taken into consideration with a modified Preisach model with seven relays in shape of parallelogram. Finally, eddy current effect is settled based on (Zhu and Knospe, 2010). Authors have shown that eddy current can be modelled with a single fractional order transfer function $E(s)$ applied on the bearing force (Eq. 3). The two parameters of the transfer function are established based on the finite element analysis of the actuator (Fig. 6). The parameters are chosen to obtain a gain of one at low frequency, and a step response (current ramp of 500A/s) with the same initial slope than the one given by FEA. Consequently, the characteristic obtained are R_0 equals one and c equals 0.053 in international units.

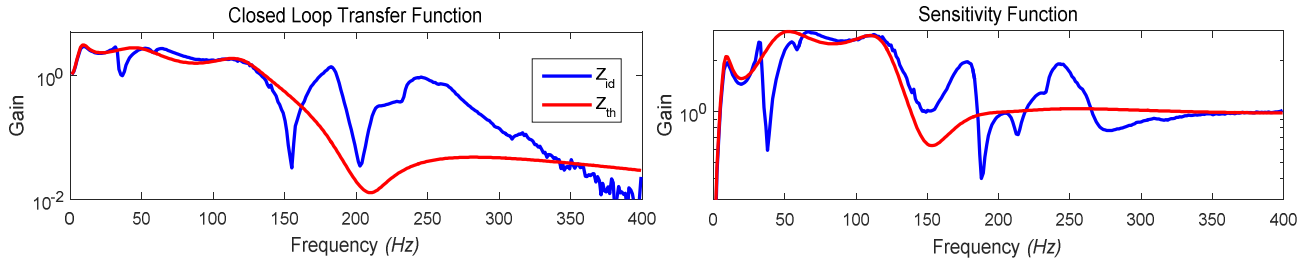

Fig. 10 Comparison between experimental (Z_{id}) and model (Z_{th}) closed loop and sensitivity transfer functions. The differences are mainly driven by the 3 stator modes not considered in the model.

$$E(s) = \frac{R_0}{R_0 + c\sqrt{s}} \tag{3}$$

Due to computation issues, the eddy current effect is imposed only on current and not on force as suggested by (Zhu and Knospe, 2010). At this stage it seems sufficient to catch the effect of eddy currents. However, authors are still in research of solutions to tackle this problem.

5. Dynamic test results

Test campaign has been executed to cover different operating cases: different bias currents, different force amplitudes and slew rates at stand still and in rotation.

Figure 11 shows the comparison between experimental results and numerical model for a large external disturbance. For this case, the bias current is set to 5A. For numerical assessment the case study is duplicated to see the effect of magnetic hysteresis (experimental data are exactly the same set replicated). The Disturbance reaches 15kN with a slew ramp of 78kN/s. From a control point of view, the current reaches a peak slew rate of 186A/s well below the amplifier capacity. Finally, the experimental maximum displacement is 117µm and the displacement computed with the model exceeds this value by 15%, what seems clearly acceptable for such a complex system.

Compared to actuator capacities, the requested forces are well below in term of amplitude and slew rate. Nevertheless, the displacement achieved is already half the backup bearing air gap. For this study, the limiting element was the control. It was impossible to increase controller gain due to casing dynamic (stator modes inside the thrust bandwidth). The thrust dynamic stiffness obtained is relatively high and consequently the support stiffness has a significant impact on thrust sensitivity function.

The improvement of actuator bandwidth should not affect directly the system performances. However, we can expect that the increase of actuator bandwidth would enable to better control structural modes and so to increase the controller gain and finally the system performances.

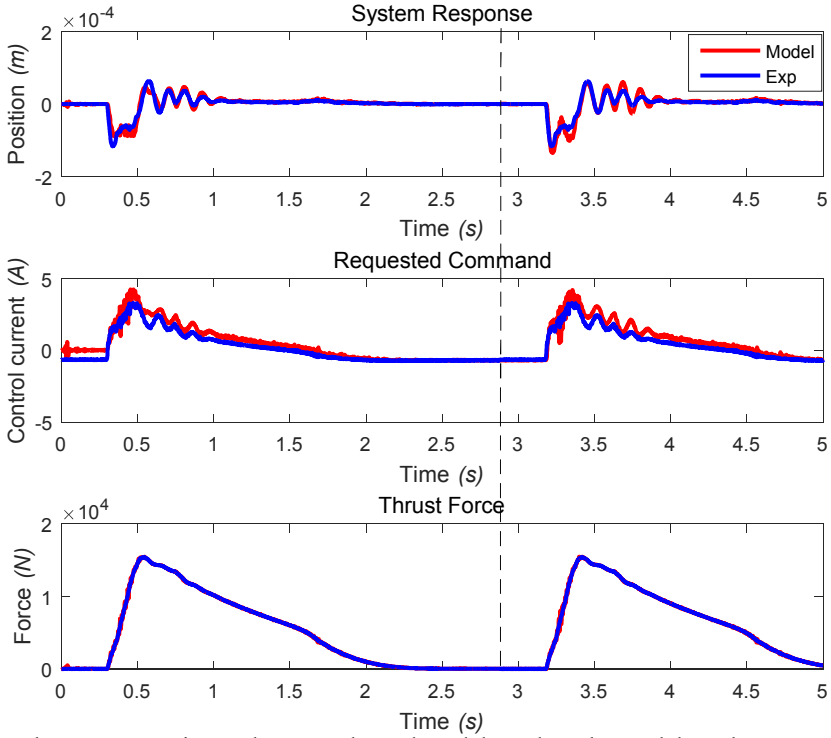

Fig. 11 Comparison between experimental test results and model results. The model catches very well the overall system dynamic. The repetition of test (numerically) enables to see the effect of magnetic hysteresis: the response depends on system history and the static control current for a nil external force is not necessarily nil.

6. Conclusions

A magnetic thrust design strategy is depicted. The thrust material is characterized experimentally and used to run magnetic finite element analysis. The step response obtained with FEA is used to set the eddy current filter parameters of a global model of bearing plus rotor. Finally, the global model allows the computation of system response to external process loads induced in turbomachinery by gas flow variations.

The design approach is validated with experimental results on an axisymmetric thrust made of a solid disk in steel and two E shape electromagnets. A good correlation is obtained between FEA and results on actuator characterization

rig showing that FEA is an interesting starting point for thrust design. Then, the thrust performance is tested on a complete system equipped with a rotor on two radial magnetic bearings. The global system model exhibits similar behavior than the one observed experimentally with 15% error on maximum displacement. These results encourage the development of system modelling in order to improve the prediction of centrifugal compressors axial dynamic behavior.

The results have permitted to highlight that the thrust performance is not necessarily limited by the actuator but by the capacity to increase the controller gain. Then, improvements can be done by following two different ways: by increasing actuator bandwidth (this will allow to better control the high frequency dynamic of the system) or by increasing the stator rigidity and consequently by pushing the structural modes out of the controller bandwidth.

This study enables better understanding of the behavior of large thrust bearings. In addition, the work realized help to predict and optimize thrust bearing responses for each machine. Indeed, before to select a thrust capacity, a control analysis could be run to identify the maximum controller gain that can be achieved. Then, based on this gain a dynamic analysis can allow to compute the maximum transient load that can be sustained. Finally, knowing the process maximum static load applied and the maximum dynamic load sustainable the thrust capacity can be selected. In the case where the process dynamic loads exceed the maximum dynamic load sustainable, the machine design must be modified.

The approach could be improved through a better modelling of the system. For example, eddy current effect modelling does not fit perfectly theory. In addition simplify model considers that the magnetic field is homogenous inside the actuator. Allowing for non-homogenous distribution should permit significant improvements.

References

Allaire, P., Fittro, R., Maslen, E. and Wakefield, W., Measured Force/Current Relations in Solid Magnetic Thrust Bearings, ASME. J. Eng. Gas Turbines Power, vol. 119(1), pp. 137-142 (1997).

API 617. Axial and centrifugal compressors and expander-compressors for petroleum, chemical and gas industry service, 8th ed. (2014).

Defoy, B., Alban, T. and Mahfoud, M., Assessment of the effectiveness of a polar fuzzy approach for the control of centrifugal compressors, J. of Dyn. Sys., Meas., and control, vol. 136, I. 4, 8p (2014).

Hijikata, K., Kobayashi, S., Takemoto, M., Tanaka, Y., Chiba, A. and Fukao, T., Basic Characteristics of an Active Thrust Magnetic Bearing With a Cylindrical Rotor Core, IEEE Transactions on Magnetics , vol. 44, no. 11, pp. 4167-4170 (Nov. 2008).

ISO 14839, Mechanical Vibration – Vibration of rotating machinery equipped with active magnetic bearings – Part 1: (2002), Part 2: (2004), Part 3: (2006).

Jang, S.-M., Lee, U.-H., Choi, J.-Y. and Hong, J.-P., Design and analysis of thrust active magnetic bearing, J. Appl. Phys., vol 103 (2008).

Li, G., Lin, Z., Allaire P. E. and & Luo J., Modelling of a high speed rotor test rig with active magnetic bearings, ASME Journal of Vibration and Acoutics, Vol. 128, Issue 3, pp. 269-271 (2006).

Maslen, E. H., Smart Machine Advances in Rotating Machinery, In IMechE, Exeter, UK, 8-10 (September 2008).

Ransom, D., Masala, A., Moore, J., Vannini, G. and Camatti, M., Numerical and Experimental Simulation of a Vertical High Speed Motorcompressor Rotor Drop onto Catcher Bearings, J. of Sys. Des. and Dyn., Vol. 3, No. 4, pp.596-606 (2009).

Schweitzer, G. and Maslen, E. H., Magnetic Bearings, Theory, Design, and Application to Rotating Machinery, Springer-Verlag, 535p (2009).

Spirig, M., Schmied, J., Jenckel, P. and Kanne, U., Three practical examples of magnetic bearing control design using a modern tool, ASME J. of Eng. for Gas Turbines and Power, Vol. 124, Issue 4, pp. 1025-1031 (2002).

Swann, M. K., Sarichev, A. P. and Tsunoda, E., A diffusion model for active magnetic bearing systems in large turbomachinery, In Proceeding 11th ISMB, Japan, pp. 380-384 (2008).

Whitlow, Z., Fittro, R. and Knospe, C., Segmented magnetic thrust bearings: analytic models and predictions of significant improvement in dynamic performance, Proceedings of ISMB14, pp. 36-41 (2014).

Zhu, L. and Knospe, C., Modeling of nonlaminated electromagnetic suspension system, IEEE Trans. Mechatronics, vol. 15, no. 1, pp. 59–69 (Feb. 2010).